Jatish Kumar, Xingzhan Wei[a], Steven J. Barrow[b], Alison M. Funston, K. George Thomas and Paul Mulvaney*

Coupled Plasmon Resonances and Gap Modes in Laterally Assembled Gold Nanorod Arrays

https://doi.org/10.1515/zpch-2018-1163
Received February 21, 2018; accepted March 14, 2018

Abstract: The assembly of metal nanocrystals offers a flexible method for creating new materials with tunable, size-dependent optical properties. Here we study the lateral assembly of gold nanorods into arrays, which leads to strong colour changes due to surface plasmon coupling. We also demonstrate the first example of gap modes in colloid systems, an optical mode in which light waves propagate in the channels between the gold rods. Such modes resonate at wavelengths which strongly depend on the gap width and length.

Keywords: chain length; gap modes; gold nanorods; lateral assembly; surface plasmons.

1 Introduction

The localised surface plasmon resonance (LSPR) in metal nanoparticles is due to the coherent oscillation of conduction electrons and is highly sensitive

[a]Current address: Chongqing Institute for Green and Intelligent Technologies, Chongqing, China
[b]Current address: RMIT, School of Applied Chemistry and Environmental Science, Melbourne, VIC 3000, Australia
***Corresponding author: Paul Mulvaney,** ARC Centre of Excellence in Exciton Science, School of Chemistry, University of Melbourne, Parkville, VIC 3010, Australia, E-mail: mulvaney@unimelb.edu.au
Jatish Kumar: CSIR – National Institute for Interdisciplinary Science and Technology, Thiruvananthapuram 695 019, Kerala, India
Xingzhan Wei and Steven J. Barrow: ARC Centre of Excellence in Exciton Science, School of Chemistry, University of Melbourne, Parkville, VIC 3010, Australia
Alison M. Funston: ARC Centre of Excellence in Exciton Science, School of Chemistry, Monash University, Clayton, VIC 3800, Australia
K. George Thomas: School of Chemistry, Indian Institute of Science Education and Research, Thiruvananthapuram (IISER-TVM), CET Campus, Thiruvananthapuram 695 016, Kerala, India

to the dimension and shape of the nanoparticle [1, 2]. The localised surface plasmons of two individual nanoparticles at small interparticle separation (i.e. interparticle separation less than 2.5 times the particle diameter), interact, primarily through dipole coupling. This leads to the generation of hybridised plasmon modes [3–6]. These hybridised plasmons have found application in techniques such as surface enhanced Raman spectroscopy (SERS), and in plasmonic waveguides [3, 7–10]. While spherical nanoparticle assemblies have been extensively investigated [11–16], there are fewer studies on the assemblies of gold nanorods. The shape anisotropy of nanorods provides the opportunity to align nanorods in different orientations in the assembly and therefore to generate unique optical features. Gold nanorods have been successfully aligned in either a lateral (side-to-side) or longitudinal (end-to-end) manner using thiol coupling chemistry. Typically investigations of these assemblies are carried out in solution and the resultant extinction spectra originating from ensembles are broad and difficult to interpret [17–19]. A convenient way to understand the origin of various bands in lateral and longitudinal assemblies of Au nanorods is by investigating these systems using single particle spectroscopy [20–22].

Recent advances in dark field spectroscopy permit the direct correlation of the nature of nanoparticles to the scattering spectra of the individual particles [23]. Funston et al. [20, 24] originally utilised this method to examine the coupling of *L* and *T* Au nanorod dimers and trimers, while Shao and colleagues [22] have investigated the angle dependence of the rod dimer scattering spectra. Kumar et al. have carried out systematic studies on the longitudinal [25] and lateral [26] coupling of Au nanorods in solution, and they also investigated the optical behaviour of longitudinally assembled Au nanorods using dark field spectroscopy [21]. Herein we investigate the plasmon coupling in laterally assembled gold nanorod arrays (from an isolated nanorod to an assembly of five nanorods), with interparticle distances smaller than 2 nm. The spectral response of the clusters to polarised light are presented and correlated with the structure of the lateral assembly to enable full understanding of their spectroscopic signature. Theoretical modelling of these arrays has also been carried out, in order to confirm the assignment of these hybrid modes. Importantly, we find the existence of a new optical mode in the arrays, which is assigned to a gap mode. While gap modes are known for interacting planar metal films, they have only been observed for colloid particles coupled to macroscopic, planar metal films [27, 28]. Gap modes have not been observed previously in pure colloid systems. Because these modes could play a decisive role in SERS and waveguiding in nanoscale systems, investigations of such modes constitutes an important direction in surface plasmon spectroscopy.

2 Experimental details

2.1 Chemicals and synthesis

Gold(III) chloride trihydrate ($AuHCl_4 \cdot 3H_2O$) (99.9+%), silver nitrate ($AgNO_3$) (≥99%), sodium borohydride ($NaBH_4$) (≥99%), (3-mercaptopropyl)-trimethoxysilane (MPS) (95%), trisodium citrate and ascorbic acid (≥99%) were purchased from Sigma Aldrich. Cetyltrimethylammonium bromide (CTAB) (98%) was purchased from Ajax Chemicals. ITO coverslips were purchased from SPI. All chemicals were used without further purification. Ultrapure water (Milli-Q) was used throughout. Au nanorods of varying aspect ratios were synthesised by following the seed mediated method reported by El-Sayed and coworkers [29].

2.2 Self-assembly

The lateral assembly (also termed side-by-side assembly) of nanorods was driven by electrostatic interaction between the positively charged CTAB on the surface of the nanorod and negatively charged citrate anions added to the solution [30]. Lateral assembly of nanorods was then achieved by adding sodium citrate (3 μM) to the Au nanorod solution (0.012 nM) in water. The lateral assembly was monitored by following changes in the extinction spectra of the nanorods in solution. Freshly prepared ITO coated glass slides functionalised with (3-mercaptopropyl)-trimethoxysilane (MPS) [31], were dipped in the Au nanorod solution at different assembly stages (times) for 10 s, then removed, rinsed thoroughly with water and dried under a flow of nitrogen (Scheme 1). Monomers and dimers were observed on glass slides prepared 5 min after the addition of citrate, whereas trimers and tetramers were observed after 15 min of the addition of linker.

2.3 Spectroscopy

The assemblies deposited on the ITO slides were characterised using correlated scanning electron microscopy (SEM) and dark-field microscopy (DFM). Assembled nanostructures were imaged using a Nova Nanolab SEM and, following identification of a structure of interest, markers were etched in the substrate in a known location using a focused ion beam. The markers allow pattern matching between the electron microscope and optical microscope [23]. The scattering spectra of the individual assemblies of interest were collected using a dark field

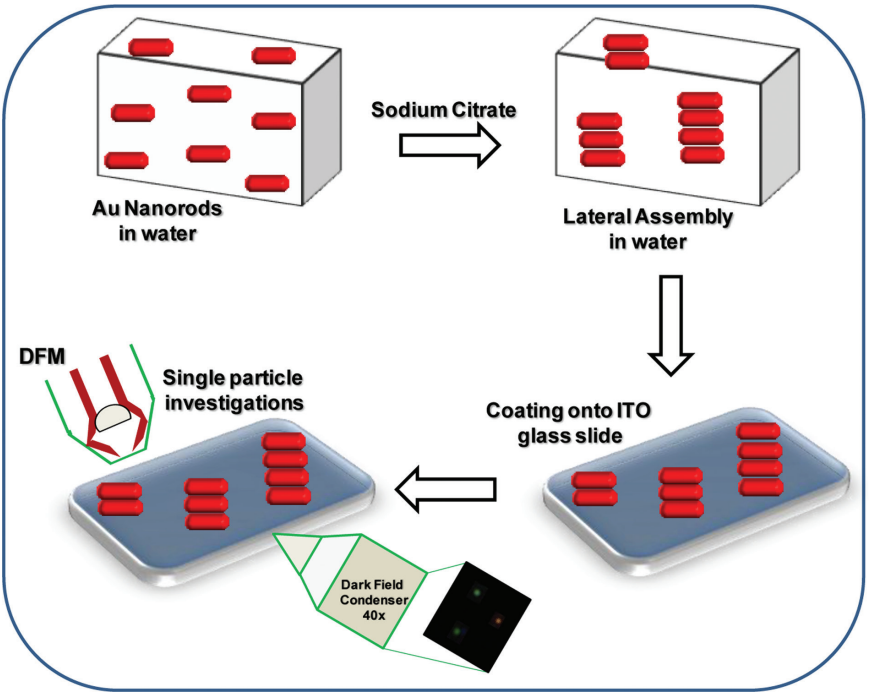

Scheme 1: Diagram illustrating the basic assembly process used.

microscope with a 0.8–0.95 NA dry dark field condenser and a Nikon Plan Fluor ELWD 40x/0.60 NA objective. The collected light was focused onto the entrance slit of a MicroSpec 2156i imaging spectrometer coupled to a TE-cooled CCD (Acton Pixis 1024). Polarised scattering spectra were collected by rotating a polariser (LPVIS 100, Thorlabs) in the light path just after the light source.

2.4 Calculations

Simulations using the finite element method (COMSOL Multiphysics v4.3) were utilised to model the optical properties of laterally assembled nanorod clusters. Details are provided in the Supporting Information.

3 Results and discussion

The basic processes used to make and assemble the gold nanorods are illustrated in Scheme 1. It is important to recognise that while the rods are assembled in

solution, the particles are transferred to a microscope slide for spectroscopic measurements. It is important to avoid aggregation during this step. SEM images and the corresponding scattering spectra obtained for the nanorod assemblies, arranged in a side-by-side fashion with an aspect ratio of ~2.3, are shown in Figure 1. For polarisation orthogonal to the interparticle axis (indicated by blue arrows), the wavelength of the surface plasmon resonance exhibits a gradual blue-shift as the number of rods in the cluster increases. The scattering spectra of single nanorods with an average length of 54 nm and width of 23 nm exhibit a plasmon resonance at 658 nm. The surface plasmon resonance blue-shifts to 640, 630, 626 and 623 nm for the dimer, trimer, tetramer and pentamer arrays, respectively (Figure 1a,f,k,p). Fits to these data reveal that the blue-shift asymptotes to a constant value of ~615 nm for more than 7–9 rods in the assembly. The calculated scattering spectra for these structures evince a similar trend (Figure 1b,g,l,q). Note that the slight variations in peak positions between the experimental and calculated spectra are due to the

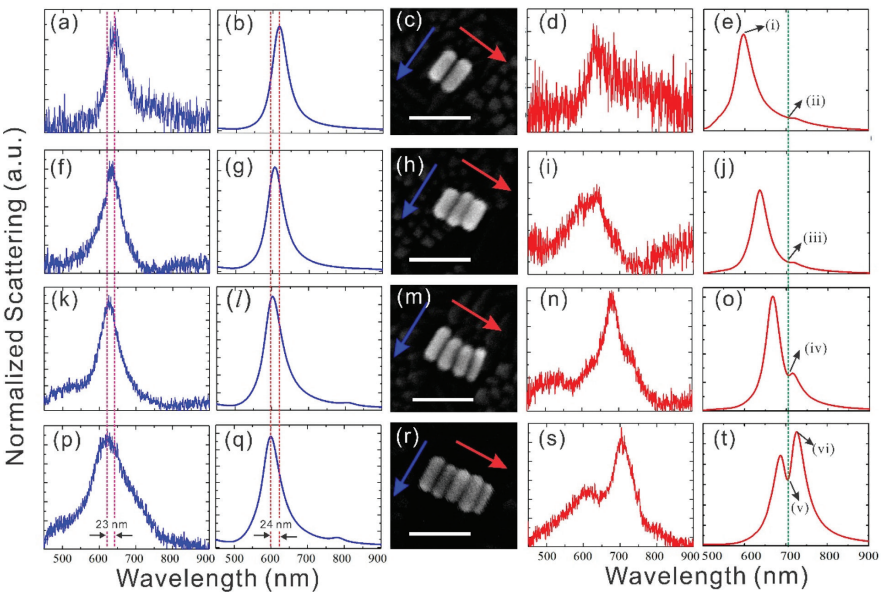

Fig. 1: Experimental and theoretical scattering spectra of Au nanorod arrays for: (left, blue traces): polarisation perpendicular to the interparticle axis; (right, red traces): parallel to the major interparticle axis. Centre: SEM images of the corresponding arrays from dimers to pentamers. FIB markers on the substrate were used as a reference for polarisation measurements. The polarisation directions (orthogonal and parallel to the interparticle axis) are indicated using blue and red arrows, respectively. All spectra were collected on ITO coated glass substrates in air. Scale bar = 200 nm.

simplifying assumption in the simulations that the interparticle spacing between the rods is 1 nm. Furthermore, a constant refractive index for the environment is assumed, whereas in the experiment, there is a large discontinuity in refractive index at the air-ITO interface. Nevertheless the calculated spectra reproduce all the experimentally observed trends. It is evident that when the polarisation is perpendicular to the interparticle axis, the longitudinal plasmons of the rods interact repulsively, resulting in "antibonding modes" that are blue-shifted relative to the longitudinal mode of individual rods. The scattering cross-section increases as the number of rods in the assembly increases yielding better signal-to-noise in the dark-field spectra. In contrast, for polarisation along the major interparticle axis (indicated by red arrows), the surface plasmon resonance exhibits a clear bathochromic shift as the number of rods in the array increases. The peak shifts from 658 nm for the dimer to 704 nm for the pentamer (Figure 1d,i,n,s). This red-shifted peak can be attributed to attractive dipolar coupling across the gap region.

Importantly, a new band emerges in the low energy region. The intensity of this lower energy resonance also increases and blue-shifts with an increasing number of rods, becoming very evident for the gold nanorod lateral-pentamer. This new mode has not been experimentally detected previously in rod assemblies due to its low scattering intensity. We attribute it to coupling of the gap mode and the bonding dipole mode. Evidence for this assignment is provided from simulations discussed below.

For polarisation of the incident light along the pentamer interparticle axis, a dip is evident in the long wavelength region of the spectra. Simulations were carried out to provide direct visualisation of the induced dipoles and the surface charge density associated with the complex optical modes. The variation in surface charge density on the surface of laterally assembled nanorods (for those peaks and dips labelled with Roman numerals in Figure 1) are presented in Figure 2. Two laterally assembled gold rods with a nanoscale gap act as a so-called metal-insulator-metal (MIM) waveguide. Gap plasmons with small wavelengths < 100 nm [32] can propagate along this interface. The plasmons supported by the narrow gaps are reflected by the rod ends, so that the electric field has a maximum at the ends, and can form standing waves in the gap. Thus, these laterally assembled clusters can be considered as Fabry-Perot resonators, the wavelengths of which are mainly decided by the gap geometry. For the same gap width and rod length, the wavelengths for the gap modes are fixed, independent of the number of particles within the cluster, as apparent from the green dashed lines in Figure 1e,j,o,t. The relevant surface charge distributions for the different clusters exhibit similar behaviour, as shown in Figure 2. The curves are marked as ii, iii, iv and v and these correspond to the dips in the spectra in Figure 1. In contrast, the resonance wavelength of the bonding dipole mode with nanometric

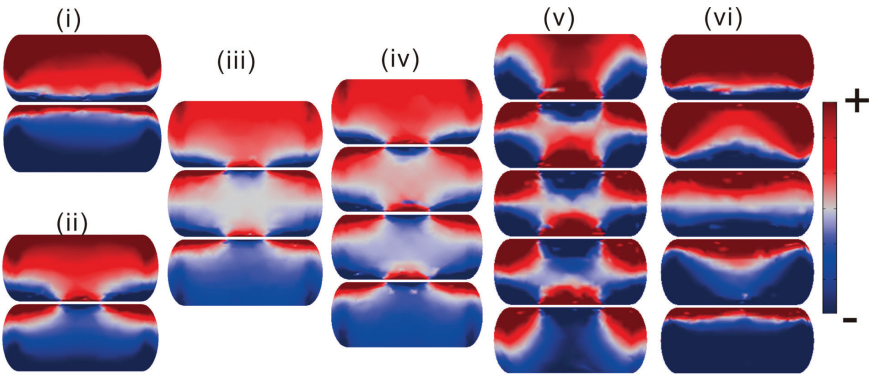

Fig. 2: Surface charge density plots for the modes associated with the dimer, trimer, tetramer and pentamer assemblies of Au nanorods for polarisation of the incident light along the interparticle axis of the laterally assembled nanorod arrays. Roman numerals correspond to specific peaks in the experimental spectra in Figure 1. Colour bar represents the charge density scale.

gaps is strongly dependent on the cluster number. The peak wavelength is 598 nm for the dimer, whereas the scattering peak of the pentamer is around 726 nm, where it overlaps with the wavelength of the gap mode. The coupling between the bonding dipole mode and the gap mode gives rise to splitting of the scattering spectrum, and it then exhibits two peaks and one dip, instead of evincing the standard Lorentz line shape.

To confirm the assignment of the scattering peaks, experiments were performed using Au nanorods possessing the same length (54 nm) but with a larger thickness (30 nm). SEM images as well as the corresponding scattering spectra of the coupled structures are shown in Figure S1. Note that while the transverse modes are still located around 520–540 nm in this sample, the longitudinal modes are blue-shifted compared to those observed for longer rods. The plasmon resonance for the dimer is observed at 605 nm for both polarisation directions, orthogonal as well as parallel to the interparticle axis (Figure S1). Interestingly, the trimeric assembly exhibits a blue shifted peak at 600 nm for polarisation orthogonal to the interparticle axis, whereas a red-shifted peak at 628 nm is observed for polarisation along the interparticle axis. Further shifts in peak positions are observed for the tetrameric assembly. The extent of the blue-shift remains almost identical in comparison to the thinner rods for polarisation perpendicular to the interparticle axis. In contrast, thick rods show more pronounced red-shifts relative to their thinner counterparts for polarisation along the interparticle axis. Hence, the blue shifted band due to the antibonding mode is less affected by the change in thickness of the nanorods, whereas the low energy mode is more sensitive to these parameters. As observed in the earlier case, good

agreement is observed between the experimental and theoretical plots, supporting the conclusion that the bonding modes arise due to attractive coupling and antibonding modes due to repulsive coupling between surface plasmon modes in individual rods. It can be concluded that the position of the low energy band is largely dependent on the thickness of the nanorods, whereas the high-energy band varies with the length of the nanorods in the laterally assembled nanostructures. Furthermore, an additional long wavelength peak becomes prominent for the tetrameric assembly, in agreement with the earlier observation.

In order to systematically analyse the gap modes, the spectra of two laterally aligned rods with different lengths and gaps have been modelled. The calculated absorption, scattering and extinction spectra for a dimer are shown in Figure S2. The extinction peak at around 678 nm is due to the gap mode. Next, we study the optical properties of dimers as a function of the nanorod length. As is evident from the calculations depicted in Figure 3a, the longer the nanorod, the greater

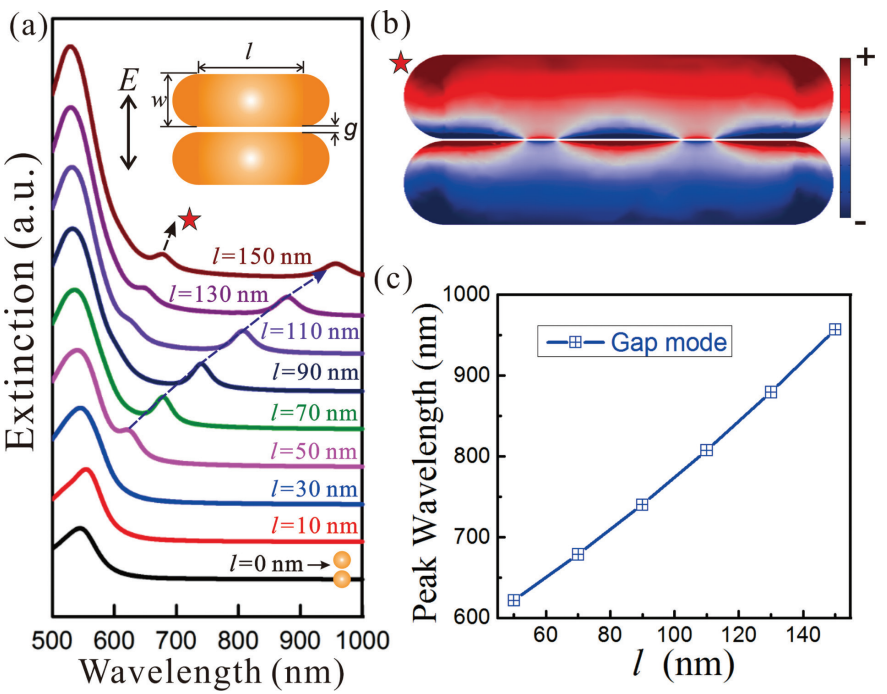

Fig. 3: (a) Calculated extinction spectra of spherically capped gold nanorods versus rod length, l (nm). (b) Surface charge distribution of the higher order gap mode. (c) Peak wavelength of first order gap mode versus length. Parameters: $w = 30$ nm, $g = 1$ nm, the permittivity of environment $\varepsilon = 1$.

the number of cavity modes that can be supported. Figure 3b shows the surface charge density associated with a high order gap mode. It is pertinent to note that the peaks of the same order exhibit an obvious red-shift as the nanorod length increases. This can be explained by the condition for surface plasmon standing waves: $l = m\lambda_{SP}/2 = m\lambda/2n_{eff}$, where m is an integer, λ_{SP} is the wavelength of the surface plasmon and λ is the free space wavelength associated with the gap mode resonance and n_{eff}, is the effective refractive index. As l increases, the corresponding resonance moves to longer wavelengths, as shown in Figure 3c.

The influence of the gap width on optical properties by varying the gap between 0.5 and 7 nm is shown in Figure 4a. The bonding mode exhibits a blue shift from 559 to 508 nm as the gap width increases (Figure 4b). Remarkably, the gap mode undergoes a much larger shift (237 nm) from 837 to 600 nm when the gap increases from 0.5 to 4 nm. Thus, the gap mode is nearly 5 times

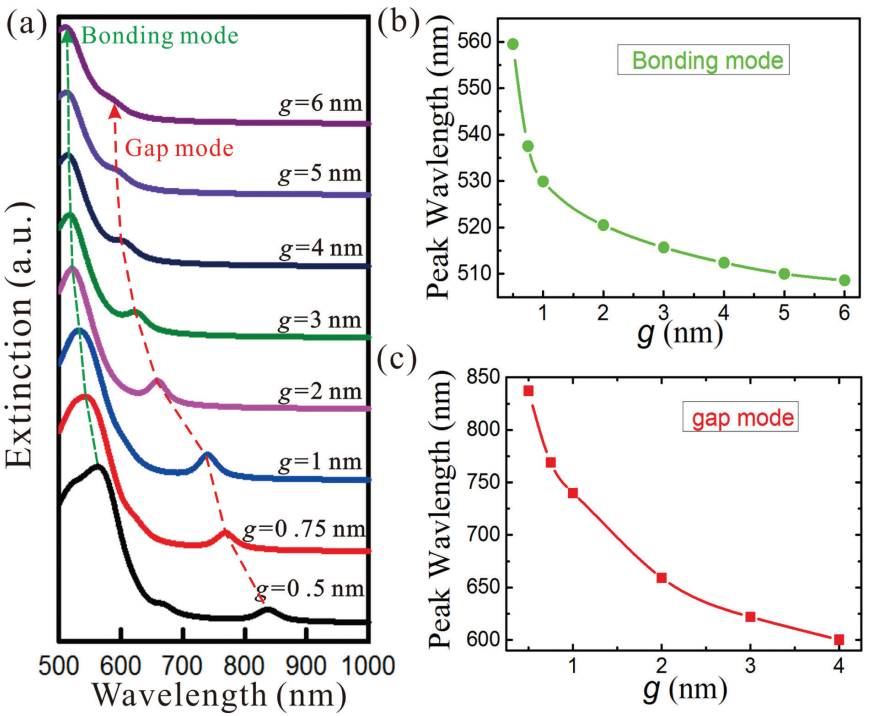

Fig. 4: (a) Calculated extinction spectra of spherically capped gold nanorods for different gap widths, g (nm). (b) Peak wavelength of the bonding mode versus gap width, g (nm). (c) Peak wavelength of the first order gap mode versus gap width, g (nm). Parameters: $w = 30$ nm and $l = 90$ nm, $\varepsilon = 1$.

more sensitive than the bonding mode. In addition, the gap mode has a sharper profile and smaller linewidth than the conventional dipole mode, which opens up new possibilities for optical sensing applications. It should be noted that the wavelength of the gap mode initially decreases rapidly, then shifts more slowly, as shown in Figure 4c. This trend can be qualitatively explained by $l = m\lambda/2n_{\text{eff}}$, in which n_{eff} exhibits an exponential decay as the gap width increases from 1 to ~10 nm [32].

4 Conclusions

In summary, using colloid chemical methods we have assembled one-dimensional nanorod structures and monitored the coupling of the SP modes using dark field spectroscopy. The light scattering properties of laterally arranged Au nanorod assemblies ranging from dimer to pentamer have been investigated and compared to modelling results obtained using FEM. The presence of bonding and antibonding modes gives rise to red- and blue-shifts respectively, as the number of rods in the arrays increases. The shift decreases with increasing rod numbers and appears to asymptote to a finite energy for about 7–9 laterally coupled gold nanorods. We have also shown that new hybridisation modes arise for higher order assemblies. These involve the propagation of light as gap modes. Molecules in the channels between these rods may couple strongly to the gap modes, providing a new method for spectroscopic detection and identification of low concentrations of adsorbed analytes.

Acknowledgements: The authors thank the ARC for support through grants LF11000117 and CE170100026.

References

1. R. Sardar, A. M. Funston, P. Mulvaney, R. W. Murray, Langmuir **25** (2009) 13840.
2. C. J. Murphy, T. K. Sau, A. M. Gole, C. J. Orendorff, J. Gao, L. Gou, S. E. Hunyadi, T. Li, J. Phys. Chem. B **109** (2005) 13857.
3. S. A. Maier, P. G. Kik, H. A. Atwater, S. Meltzer, E. Harel, B. E. Koel, A. A. G. Requicha, Nat. Mater. **2** (2003) 229.
4. W. L. Barnes, A. Dereux, T. W. Ebbesen, Nature **424** (2003) 824.
5. N. J. Halas, Nano Lett. **10** (2010) 3816.
6. M. Quinten, A. Leitner, J. R. Krenn, F. R. Aussenegg, Opt. Lett. **23** (1998) 1331.
7. L. Vigderman, B. P. Khanal, E. R. Zubarev, Adv. Mater. **24** (2012) 4811.

8. S. Eustis, M. A. El-Sayed, Chem. Soc. Rev. **35** (2006) 209.
9. J. Huang, L. Zhang, B. Chen, N. Ji, F. Chen, Y. Zhang, Z. Zhang, Nanoscale **2** (2010) 2733.
10. S. A. Maier, M. L. Brongersma, P. G. Kik, S. Meltzer, A. Requicha, B. E. Koel, H. A. Atwater, Adv. Mater. **13** (2001) 1501.
11. S. J. Barrow, A. M. Funston, D. E. Gomez, T. J. Davis, P. Mulvaney, Nano Lett. **11** (2011) 4180.
12. Y. Ofir, B. Samanta, V. M. Rotello, Chem. Soc. Rev. **37** (2008) 1814.
13. D.-K. Lim, K.-S. Jeon, H. M. Kim, J.-M. Nam, Y. D. Suh, Nat. Mater. **9** (2010) 60.
14. W. Li, P. H. C. Camargo, X. Lu, Y. Xia, Nano Lett. **9** (2009) 485.
15. S. J. Barrow, A. M. Funston, X. Wei, P. Mulvaney, Nano Today **8** (2013) 138.
16. S. J. Barrow, D. Rossouw, A. M. Funston, G. A. Botton, P. Mulvaney, Nano Lett. **14** (2014) 3799.
17. K. K. Caswell, J. N. Wilson, U. H. F. Bunz, C. J. Murphy, J. Am. Chem. Soc. **125** (2003) 13914.
18. P. Pramod, K. G. Thomas, Adv. Mater. **20** (2008) 4300.
19. K. Liu, Z. Nie, N. Zhao, W. Li, M. Rubinstein, E. Kumacheva, Science **329** (2010) 197.
20. A. M. Funston, C. Novo, T. J. Davis, P. Mulvaney, Nano Lett. **9** (2009) 1651.
21. J. Kumar, X. Wei, S. Barrow, A. M. Funston, K. G. Thomas, P. Mulvaney, Phys. Chem. Chem. Phys. **15** (2013) 4258.
22. L. Shao, K. C. Woo, H. Chen, Z. Jin, J. Wang, H.-Q. Lin, ACS Nano **4** (2010), 3053.
23. C. Novo, A. M. Funston, I. Pastoriza-Santos, L. M. Liz-Marzan, P. Mulvaney, Angew. Chem. Int. Ed. **46** (2007) 3517.
24. A. M. Funston, T. J. Davis, C. Novo, P. Mulvaney, Phil. Trans. R. Soc. A **369** (2011) 3472.
25. J. Kumar, K. G. Thomas, J. Phys. Chem. Lett. **2** (2011) 610.
26. J. Kumar, R. Thomas, R. S. Swathi, K. G. Thomas, Nanoscale **6** (2014) 10454.
27. A. Lombardi, A. Demetriadou, L. Weller, P. Andrae, F. Benz, R. Chikkaraddy, J. Aizpurua, J. J. Baumberg, ACS Photonics **3** (2016) 471.
28. B. de Nijs, F. Benz, S. J. Barrow, D. O. Sigle, R. Chikkaraddy, A. Palma, C. Carnegie, M. Kamp, R. Sundararaman, P. Narang, O. A. Scherman, J. J. Baumberg, Nat. Commun. **8** (2017) Article 994.
29. B. Nikoobakht, M. A. El-Sayed, Chem. Mater. **15** (2003) 1957.
30. A. McLintock, N. Hunt, A. W. Wark, Chem. Commun. **47** (2011) 3757.
31. M. B. Ali, F. Bessueille, J. M. Chovelon, A. Abdelghani, N. Jaffrezic-Renault, M. A. Maaref, C. Martelet, Mater. Sci. Eng. C **28** (2008) 628.
32. H. T. Miyazaki, Y. Kurokawa, Phys. Rev. Lett. **96** (2006) 097401.

Supplemental Material: The online version of this article offers supplementary material (https://doi.org/10.1515/zpch-2018-1163).